

# Development of Phase-Separated Scintillators with Light-Guiding Properties and their Application for High-Resolution X-ray Imaging

著者	大橋 良太
号	59
学位授与機関	Tohoku University
学位授与番号	工博第5022号
URL	<a href="http://hdl.handle.net/10097/62776">http://hdl.handle.net/10097/62776</a>

氏 名	おお はし よし ひろ
授 与 学 位	大 橋 良 太
学位授与年月日	博士 (工学)
学位授与の根拠法規	平成26年9月24日
研究科, 専攻の名称	学位規則第4条第1項
学 位 論 文 題 目	東北大学大学院工学研究科 (博士課程) 材料システム工学専攻
	Development of Phase-Separated Scintillators with Light-Guiding Properties and their Application for High-Resolution X-ray Imaging.
	(光導波機能を有する相分離シンチレータ材料の開発と高分解能X線イメージングへの応用に関する研究)
指 導 教 員	東北大学教授 吉川 彰
論 文 審 査 委 員	主査 東北大学教授 吉川 彰 東北大学教授 後藤 孝
	東北大学教授 山根 久典 東北大学教授 増本 博

## 論文内容要旨

### Chapter 1. Introduction

In high-resolution radiation imaging systems based on inorganic scintillators, a scintillation light must be guided to the photo-sensors efficiently without lateral light diffusion to achieve the high resolution imaging. Future X-ray imaging applications require a higher spatial resolution with micrometer scale over a wide X-ray energy range. Particularly indirect flat panel detector, which is composed of a scintillator layer and photo-sensor array, requires improvements in their sensitivity and spatial resolution. High sensitivity can be achieved by using a sufficiently thick scintillator layer to absorb the incident X-ray energy completely. However, conventional scintillators, such as  $\text{Gd}_2\text{O}_2\text{S:Tb}$  (GOS) powder screens, and even CsI:Tl columnar films reduce the spatial resolution because increasing the thickness causes more light scattering due to the insufficient separation between columns as well as their sidewall roughness. To achieve high sensitivity compatible with high-resolution imaging over a wide radiation energy range, the scintillator layer must possess perfect light guiding properties.

In this study, a new concept of a phase-separated scintillator (PSS) with ideal light guiding property is proposed. The PSS is composed of regular directionally solidified eutectic (DSE) materials with unidirectionally aligned smooth cylinders embedded in a matrix phase. The cylinders usually grow vertically on a solid-liquid interface, and these uniform structures are expected to guide light effectively. The main purpose of this thesis is to develop various PSSs with effective light-guiding properties and to demonstrate a high-resolution X-ray imaging by using them.

### Chapter 2. Concept of the Phase-Separated Scintillator (PSS)

This chapter described the capability of a concept of the PSS by simulations. The light-receiving efficiency for various refractive indices of the cylinders and matrix were calculated from the light flux collection efficiencies of the emitted light. From the calculations, two types of possible PSSs were suggested owing to the refractive index ratio ( $n_m/n_c$ ) of the cylinders ( $n_c$ ) and the matrix ( $n_m$ ): matrix-guided PSSs ( $n_m/n_c > 1$ ) and cylinder-guided PSSs ( $n_m/n_c < 1$ ). In the both types, the scintillation lights were transported along the cylinder direction by optical reflection with a total reflection mode between the smooth boundaries with different refractive indices, and the light-guiding efficiency increased as increasing the refractive index ratio ( $n_m/n_c$ ). In the matrix-guided PSSs, scintillation light was guided in the matrix phase with higher refractive index, so that the emitted light was partly diffused in the matrix phase due to its continuous structure, and the high volume fraction of the cylindrical phase was important for improving the light guiding efficiency because it produced sufficient multiple reflections.

Whereas, the cylinder-guided PSS had light-guiding properties confined to the cylinders, so that it had better light-guiding property than matrix-guided PSSs because of its strictly confined light-guiding behavior like an optical fiber.

### Chapter 3. Matrix-guided PSSs

This chapter described the fabrication of various matrix-guided PSSs and the X-ray imaging results by using them. Various matrix-guided PSSs were fabricated from alkali halide based DSEs. Among them, the CsI-NaCl PSS (CsI:NaCl = 69:31 mol%) consists of the CsI scintillator matrix ( $n \approx 1.79$ ) and NaCl cylinders ( $n \approx 1.54$ ) was a potential matrix-guided PSS because the CsI matrix phase works as an effective scintillator and its fabrication feasibility. A schematic of the CsI-NaCl PSS is shown in Fig.1(a) and prepared CsI-NaCl eutectic is shown in Fig.1(b). Characters beneath the sample were guided to the sample surface because lights were guided along the straight cylinders oriented normal to the surface. An optical transmission images is shown in Fig.1(c). The CsI matrix appeared brighter than the NaCl cylinders because CsI matrix with high refractive index guide light from the back of the crystal to the front. By using Czochralski method, Tl-doped CsI-NaCl PSS crystal that was uniform with no grain boundaries greater than 30 mm in diameter was successfully grown by creating a convex solid/liquid interface, selecting a single grain, and increasing the diameter of the composite moderately.

In addition, the porous cuprous iodide (CuI) scintillator containing aligned cylindrical micropores with a volume fraction of 30% was fabricated by leaching the Cu/KCl PSS (CuI:KCl = 73:27 mol%) in water. The KCl cylinders readily dissolve in water, whereas the CuI matrix is insoluble, therefore cylinder phases were selectively removed by immersing in water. The porous CuI is one of the matrix-guided PSSs and it behaved as efficient light waveguide scintillators due to its high refractive index ratio ( $n_m/n_c \approx 2.35$ ).

A X-ray imaging of a resolution chart of 0.05-mm-thick lead with a 10 line-pairs/mm (lp/mm) pattern was demonstrated by using a CsI-NaCl:Tl PSS and porous CuI scintillator. Contrast transfer function (CTF) values of 10 line-pairs (lp)/mm were 6% for a 420- $\mu$ m-thick CsI-NaCl:Tl PSS, while the 30% pore volume porous CuI showed better CTF value of 11% for a 800- $\mu$ m-thick sample. This CTF value of the porous CuI might be the limit of the matrix-guided PSSs because it has relatively higher refractive index ratio and higher volume fraction of cylinder phases than other matrix-guided PSSs.

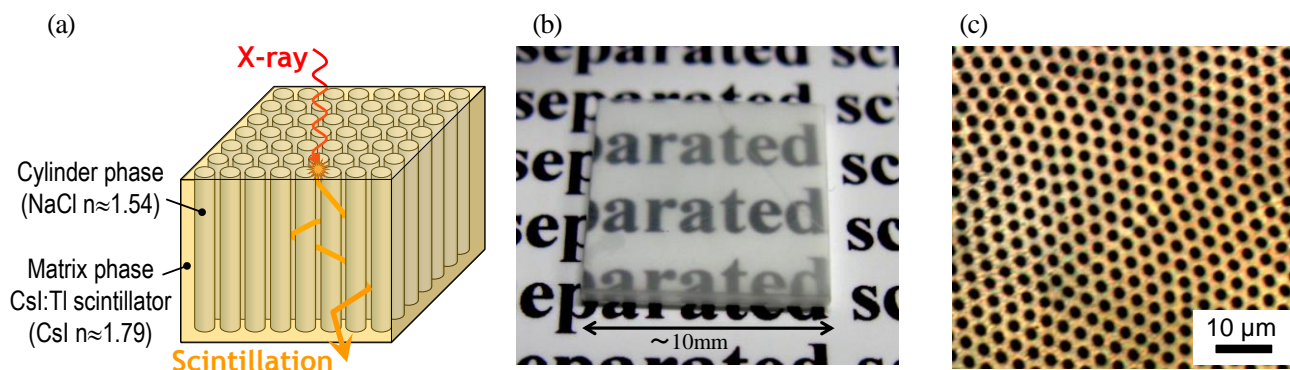


Fig.1. Matrix-guided CsI-NaCl PSS: (a) Schematic illustration, (b) appearance of the CsI-NaCl eutectic crystal, and (c) optical transmission microscope image.

### Chapter 4. Cylinder-guided GAP-Al<sub>2</sub>O<sub>3</sub> PSS

This chapter described the fabrication of a cylinder-guided GdAlO<sub>3</sub> (GAP [gadolinium aluminum perovskite])-Al<sub>2</sub>O<sub>3</sub> PSS and its structural, luminescence and optical properties were investigated. A cylinder-guided Ce<sup>3+</sup>-doped GAP-Al<sub>2</sub>O<sub>3</sub> PSS (GAP:Al<sub>2</sub>O<sub>3</sub> = 46:54 mol%) consists of the hexagonally well-aligned 680-nm-diameter GAP:Ce<sup>3+</sup> scintillator cylinders surrounded with  $\alpha$ -Al<sub>2</sub>O<sub>3</sub> was successfully fabricated by maintaining the orientation relationship between the *c*-axis of Al<sub>2</sub>O<sub>3</sub> matrix and the growth direction of unidirectional solidification. A schematic of the GAP-Al<sub>2</sub>O<sub>3</sub>

PSS is shown in Fig.2(a) and its appearance and microstructure are shown in Fig.2(b). The GAP scintillator cylinders have a higher refractive index ( $n \approx 2.05$ ) than surrounding  $\text{Al}_2\text{O}_3$  matrix ( $n \approx 1.79$ ), so that they served as an optical fiber with multi-mode guiding of visible light as shown in Fig.2(c). The image of the lines beneath the sample appears to float on the top surface of the sample, like a fiber optic plate. When irradiated with X-rays, the GAP scintillator cylinders convert X-rays to light, and emitted light is confined and transported along the cylinder direction in the total reflection mode between GAP/ $\text{Al}_2\text{O}_3$  boundaries without light-scattering.

The structural analyses revealed that the majority of GAP cylinders had the orientation relationships of  $[010]\text{GAP}/[0001]\text{Al}_2\text{O}_3$  to the growth direction and  $(100)\text{GAP}/(1120)\text{Al}_2\text{O}_3$  to the interface plane, while slight misorientation angle of both  $[010]\text{GAP}$  axis and  $(100)\text{GAP}$  plane were observed. The EBSD orientation maps is shown in Fig.2(d). The misorientation of each GAP cylinder could be explained by the other sets of preferable lattice matching between the two phases. The tilt of  $[010]\text{GAP}$  axis toward the  $[001]\text{GAP}$  direction could be derived from the competition between  $(020)\text{GAP}/(0006)\text{Al}_2\text{O}_3$  and  $(022)\text{GAP}/(0006)\text{Al}_2\text{O}_3$ . The rotation of  $(100)\text{GAP}$  plane could be derived from the competition between  $(100)\text{GAP}/(1120)\text{Al}_2\text{O}_3$  and  $(101)\text{GAP}/(0110)\text{Al}_2\text{O}_3$ . A few observed minor orientations could be also explained by the other preferable lattice matching. In the GAP/ $\text{Al}_2\text{O}_3$  interface, a relatively large lattice misfit between the two phases was relieved by insertion of extra half-planes on the  $\text{Al}_2\text{O}_3$  side of the interface. These structural analyses indicate that the essential growth parameter for the fabrication of a GAP/ $\text{Al}_2\text{O}_3$  eutectic composite with well-aligned fibrous microstructure is the correspondence between the  $c$ -axis of  $\text{Al}_2\text{O}_3$  matrix and the growth direction of unidirectional solidification.

The cathodoluminescence (CL) spectra of individual GAP cylinders showed typical 5d-4f emission band of  $\text{GAP}:\text{Ce}^{3+}$ , while their spectral shape and emission peak showed evident variations. It is considered that these emission variations could be originated from the different orientation relationship of GAP cylinders with  $\text{Al}_2\text{O}_3$  matrix, which induces slight lattice distortion and changes in the local crystal-field strength of  $\text{Ce}^{3+}$ , and consequently emission band variations were emerged. Whereas, the CL spectra of  $\text{Al}_2\text{O}_3$  phase showed intrinsic  $\text{F}^+$ -center emission, however, its emission was not observed in radioluminescence spectrum of a bulk eutectic composite due to mainly the low attenuation coefficient of  $\text{Al}_2\text{O}_3$  phase, additionally the spectral overlapping between emission band of  $\text{F}^+$ -center and excitation/emission bands of GAP phase.

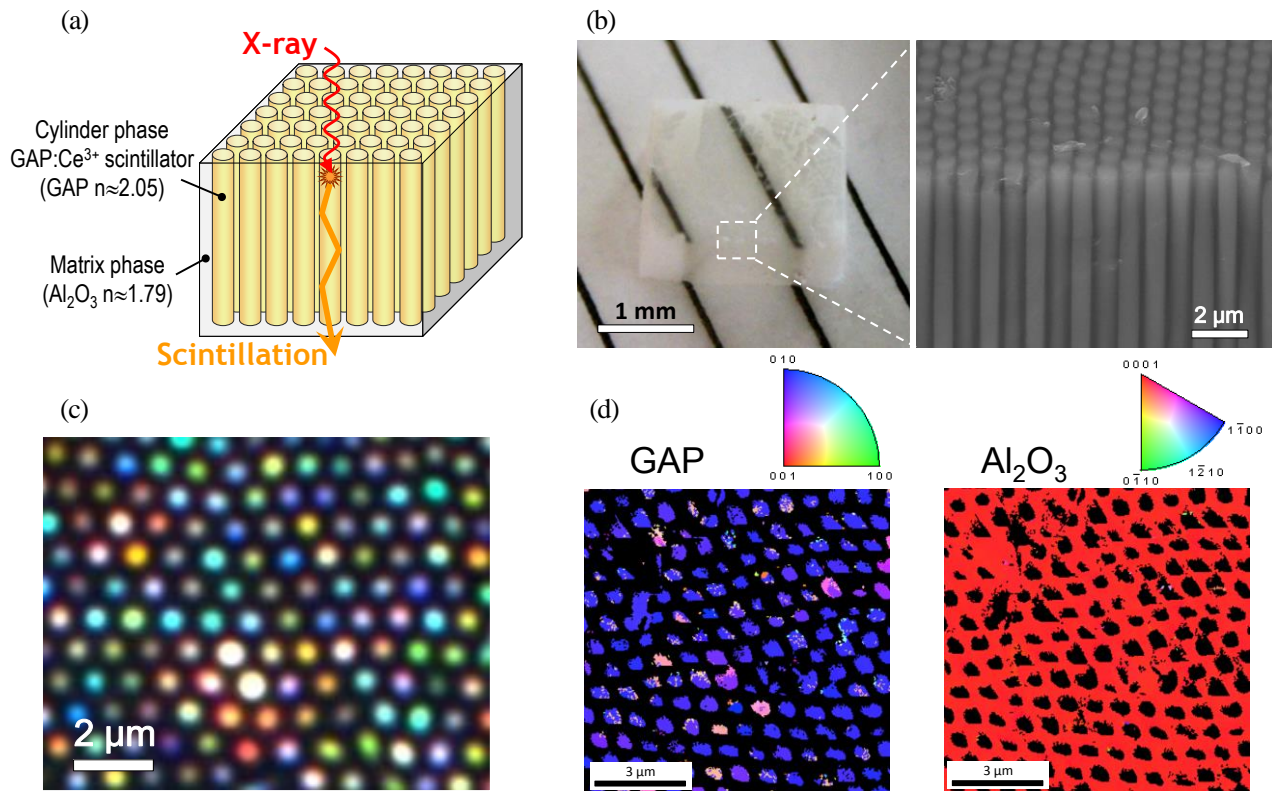


Fig.2. Cylinder-guided GAP- $\text{Al}_2\text{O}_3$  PSS: (a) Schematic illustration, (b) appearance and microstructure of the eutectic crystal (c) optical transmission microscope image, and (d) EBSD orientation maps.

## Chapter 5. Demonstration of high-resolution X-ray imaging with a GAP- $\text{Al}_2\text{O}_3$ PSS

This chapter described the high-resolution X-ray imaging results demonstrated by using the  $\text{Ce}^{3+}$ -doped GAP- $\text{Al}_2\text{O}_3$  PSS. The relationship between the CTF values at 10 lp/mm and the thickness is shown in Fig.3(a). The CTF values of the conventional GOS powder screen (88, 180  $\mu\text{m}$  thick) and the CsI:Tl columnar film (150, 180, 300, 550  $\mu\text{m}$  thick) were also shown for comparison. For the GOS powder screen, the CTF values decreased sharply as the thickness increased, because of strong light scattering. Even though the CsI columnar film had better light guiding properties, the CTF values decreased as the thickness increased, because of the light scattering caused by the surface roughness or imperfections in the crystal. No contrast was observed for samples thicker than 500  $\mu\text{m}$ . Thus, the conventional scintillator suffered from a resolution reduction as its thickness increased because of light scattering. In contrast, the GAP- $\text{Al}_2\text{O}_3$  PSS achieved an extremely high resolution, even for scintillators thicker than 1 mm, because of the excellent light guiding properties by the total reflection mode.

Finally, a micrometer-scale resolution X-ray imaging was demonstrated by imaging the gold grating phantoms with a micrometer scale aperture for 150- $\mu\text{m}$ -thick sample as shown in Fig.3(b). The gold grating phantoms had aperture-pitch sizes of 9-22  $\mu\text{m}$  and 4-8.2  $\mu\text{m}$ , respectively. The 9  $\mu\text{m}$  aperture was clearly resolved, and ultimately the 4  $\mu\text{m}$  aperture, corresponding to a bundle of 12 GAP cylinders, was resolved but with low-contrast. The low contrast for the 4  $\mu\text{m}$  aperture can be explained by the propagation of primary photoelectrons and reabsorption of secondary radiation away from the initial position of incident X-ray, and some defects of GAP- $\text{Al}_2\text{O}_3$  PSS. This result indicates that GAP- $\text{Al}_2\text{O}_3$  PSS may reach the physical resolution limit determined by the material itself.

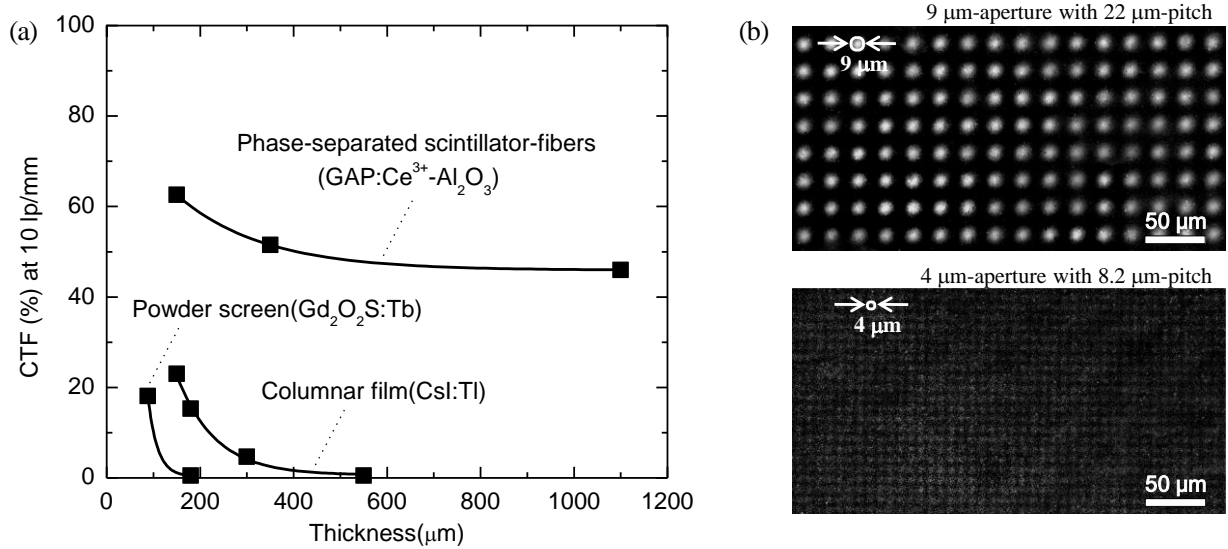


Fig.3. High-resolution X-ray imaging results. (a) CTF values at 10 lp/mm for GAP: $\text{Ce}^{3+}$ - $\text{Al}_2\text{O}_3$  PSS with various thicknesses. (b) X-ray images of gold grating phantoms with aperture-pitch sizes of 9-22  $\mu\text{m}$  and 4-8.2  $\mu\text{m}$  obtained using a 150  $\mu\text{m}$  thick GAP: $\text{Ce}^{3+}$ - $\text{Al}_2\text{O}_3$  PSS.

## Chapter 6. Conclusion

From this study, various matrix-guided and cylinder-guided PSS were developed from eutectic pairs consist of scintillator materials. Especially, the cylinder-guided GAP- $\text{Al}_2\text{O}_3$  PSS enable high-resolution X-ray imaging with micrometer scale regardless of its thickness due to its strictly confined light-guiding behavior in the cylinder phases like an optical fiber. The X-ray imaging system composed of the GAP- $\text{Al}_2\text{O}_3$  PSS and miniaturized photo-sensor arrays with micrometer scale pitch can be potentially used for future X-ray imaging applications which require a higher spatial resolution over a wide X-ray energy range.

# 論文審査結果の要旨

本研究は光導波機能を有する相分離シンチレータ材料の開発と高分解能X線イメージングへの応用に関する研究であり、全6章からなる。

シンチレータを用いた放射線検出器は、陽電子放出断層撮影 (PET)、X線コンピュータ断層撮影 (X線CT) 等の医療分野あるいは手荷物検査等の保安分野等において広く用いられている。近年の放射線利用技術の発展に伴い放射線検出器には、より高度な性能が求められている。本研究では、この検出器の高分解能化を目指し、シンチレータとシンチレータでなく屈折率の低い酸化物を組み合わせた共晶体の作製と特性評価を行った。

第1章は、序論であり、本研究の背景と目的を述べている。

本研究では共晶体を作製することが可能な形状制御結晶成長法であるマイクロ引下げ法 ( $\mu$ -PD 法) およびをチョクラルスキー法 (Cz 法) 用いて試料作製を行った。シンチレータ材料の評価としては、走査型電子顕微鏡、透過型電子顕微鏡、紫外線励起発光スペクトル測定装置、カソードルミネッセンス、波高値スペクトル測定装置等を活用した。試料の分解能評価としてはCMOSと組み合わせた評価も行った。

第2章では、相分離型シンチレータの概念について述べている。2相の屈折率がどのような相対関係にある時に有効であるかなどを議論した。

第3章では、マトリックス導波型相分離型シンチレータの実験結果について述べている。CsI-NaCl:Tl や CuI-KCl など、主にアルカリハライドを含む共晶体の時にマトリックス導波型となる。10mm角のマトリックス導波型相分離型シンチレータが得られた。

第4章では、シリンダ導波型相分離型シンチレータの実験結果について述べている。まず、GAP- $\text{Al}_2\text{O}_3$  においてシリンダ型が均質な分布を示す際の2相の方位関係を明らかにした。成長方向に  $[010]\text{GAP} // [0001]\text{Al}_2\text{O}_3$  の関係、界面において  $(100)\text{GAP} // (11\bar{2}0)\text{Al}_2\text{O}_3$  の時に安定となるという知見が得られた。放射線励起に対する発光も得られ、当該材料がシリンダ導波型相分離型シンチレータとして動作することが明らかとなった。

第5章では、シリンダ導波型相分離型シンチレータである GAP- $\text{Al}_2\text{O}_3$  を用いて分解能評価を行った。4ミクロンの分解能が得られること、更にシンチレータ相が厚くなっても劣化が少ないことなどが明らかとなった。

第6章では、上記をまとめた。

以上、要するに本論文は、酸化物共晶体を世界で初めて相分離型シンチレータとして活用できることを提案し、実際に作製し、分解能評価も行うことで実証したもので、次世代放射線検出器の開発については放射線利用技術の発展に寄与するところが少なくない。

よって、本論文は博士(工学)の学位論文として合格と認める。